PHILOSOPHICAL TRANSACTIONS OF THE ROYAL SOCIETY A MATHEMATICAL, PHYSICAL & ENGINEERING SCIENCES

Dynamic Thermal Stresses in a Pulsed Reactor

E. W. Parkes and G. A. Carter

Phil. Trans. R. Soc. Lond. A 1971 **270**, 325-347
doi: 10.1098/rsta.1971.0077

DYNAMIC THERMAL STRESSES IN A PULSED REACTOR

By E. W. PARKES and G. A. CARTER
Cambridge University Engineering Laboratory

(*Communicated by Sir John Baker, F.R.S.—Received* 11 *January* 1971)

[Plate 11]

CONTENTS

The paper begins by considering the reasons why dynamic thermal stresses are rarely encountered and then goes on to discuss the three means by which they may most readily be produced: large electric currents, impulsive electromagnetic radiation and neutron bombardment of fissile material. This is followed by a brief description of the U.K.A.E.A. pulsed reactor Viper (the design studies for which were the starting-point of the present work) and by theoretical solutions for the elastic displacements and stresses in slender cylinders and cones when rapidly heated.

The paper then discusses the physical properties of enriched uranium and goes on to describe experiments on cylinders and cones of this material when subjected to large neutron pulses in Viper, including the problems of measurement in the hostile environment. Agreement between the theoretical and experimental displacements is good.

Introduction

Almost all of the stress phenomena associated with the rapid heating of solids, from the shattering of a glass placed in hot water to the kinetic heating of space vehicles re-entering the atmosphere, are essentially static. The stresses can be calculated correctly at any instant of time by imagining the body to be at rest under the instantaneous temperature field, and no significant error is caused

Vol. 270. A. 1205. (Price £0.70; U.S. $1.80) 23 [Published 14 October 1971]

by the neglect of inertia effects. Rapid heating or cooling of solids, particularly in situations where damage may occur, such as in turbine blades during starting or stopping, is commonly referred to as 'thermal shock', but the phrase is something of a misnomer, since no 'shock' in the dynamic sense occurs.

The reason why inertia effects are not important in situations such as those described above may be seen by considering a simple example. Imagine a uniform rod of length l, fixed at one end, made from a material of density ρ, Young modulus E, coefficient of linear expansion α and yield stress σ_y. Let the rod be subjected to a rate of temperature rise β. Then it may readily be shown that the maximum stress which occurs in the rod is $\beta\alpha l E^{\frac{1}{2}}\rho^{\frac{1}{2}}$.† We have to compare this with the yield stress σ_y, and so a convenient measure of significant inertia effects is that $\beta\alpha l E^{\frac{1}{2}}\rho^{\frac{1}{2}}\sigma_y^{-1}$ must not be negligible compared with unity. Insertion of typical dimensions and material properties in this criterion shows that heating rates of the order of 10^4 to 10^6 K/s are required to produce dynamic thermal stresses. Heating rates as high as these are not commonly produced by the usual processes of heat transfer through fluid motion or combustion. They may, however, be caused by the passage of large electric currents, by impulsive electromagnetic radiation, or in fissile materials by neutron bombardment.

The production of dynamic thermal stresses by electric currents has been considered both theoretically and experimentally by Krawarik & Sexl (1966). They discharged a capacitor bank through a 100 mm long × 0.8 mm diam. copper wire held at one end, and measured the motion of the free end. The electric current had a damped oscillatory form with a peak value of about 30 kA. The heating rate was in excess of 10^6 K/s and agreement between theory and experiment was good. A similar technique has been used by Austin & Parker (1967) to determine the dynamic elastic modulus at elevated temperatures.

A number of authors have given analytical solutions corresponding to impulsive electromagnetic radiation. Danilovskaya (1950) considered an elastic half-space subjected to sudden heating of its boundary. She found that the stress at a given point rose to a certain compressive value and then changed suddenly to tension as an elastic wave from the surface reached it. In a later paper Danilovskaya (1952) used a finite heat transfer coefficient at the surface and also considered the effect of thermal conductivity. The general pattern of behaviour was similar to that for the previous case, except that the change from compression to tension occurred more smoothly. Michaels (1958) considered a slender bar in which the temperature varied linearly with time and decayed exponentially with distance from one end: he found that a stress wave with a sharp peak was propagated along the bar. Michaels obtained his solution by using Fourier transforms. Zaker (1965) produced the same result by the method of characteristics: his particular interest was in microwave pulse generators. Suvorov (1963) discussed a semi-infinite bar, subjected to sudden heating of one end, in which the coefficient of thermal conductivity was temperature dependent, and in a second paper (1964) he considered a linear temperature rise of the end. Suvorov found that waves of strong discontinuity occurred if the velocity of propagation of heat was similar to that of propagation of elastic or plastic waves. Renner & Sharma (1966) considered the stresses in an ablating bar subjected to laser radiation by a modification of Michaels analysis. Hegemier & Morland (1967) introduced viscosity effects for the half space subjected to impulsive electromagnetic radiation. Like the previous authors they found that the

† The stress at time t at distance x from the fixed end of the rod is

$$-\frac{8\beta\alpha l E^{\frac{1}{2}}\rho^{\frac{1}{2}}}{\pi^2}\sum_{n=1,3,5\ldots}\frac{\cos\left(\frac{1}{2}n\pi x/l\right)}{n^2\sin\left(\frac{1}{2}n\pi\right)}\sin\left(\frac{n\pi}{2}\frac{t}{l}\sqrt{\frac{E}{\rho}}\right).$$

PHILOSOPHICAL TRANSACTIONS OF THE ROYAL SOCIETY A MATHEMATICAL, PHYSICAL & ENGINEERING SCIENCES

characteristic behaviour was a compression wave followed by a tension wave. Viscosity had little effect on the initial compression wave, but could reduce the subsequent tension wave considerably. Morland (1969*a*, *b*) discussed elasto-plastic waves due to laser radiation and Percival & Cheney (1969) described experiments on a laser-heated glass rod.

Impulsive electromagnetic radiation produces heating of a surface layer. Neutron bombardment of fissile material produces heating (generally non-uniform) throughout the mass. Papers which discuss the fundamental thermoelastic theory include Jeffreys (1930), Lessen (1956, 1957), Sneddon (1959), Eason & Sneddon (1959) and Chadwick (1962). Papers related to specific problems include two by Randles (1966*a*, *b*) on the stability of the proposed Euratom Sora reactor and one by Randles & Jaarsma (1967) on stress waves in the fuel rods of the Sora reactor; no detailed solutions are given. Serdyukova (1970) considers radial displacements in a rapidly heated cylinder of infinite length.

The present paper is concerned with an analysis of the dynamic thermal stresses and displacements in slender cylinders and cones subjected to non-uniform heating, and with experiments on cylinders and cones of fissile material carried out in the U.K.A.E.A. pulsed reactor Viper. The original stimulus for the work came from the design of the reactor itself. As will be explained in more detail in § 1, the termination of the neutron pulse is determined in part by the thermal expansion of the fuel rods. Owing to the very large heating rates this expansion may differ from that which would obtain under quasi-static conditions. In 1965 one of the authors (E. W. P.) was asked to advise U.K.A.E.A. on this problem and the analysis for slender cylinders was developed at that time. After the reactor was commissioned in 1967 the opportunity was taken to carry out experiments on fissile specimens and the analysis was extended as outlined in § 2 to include slender cones as a means of increasing the dynamic stress levels. It was hoped that some of the tests on slender cones would produce inelastic behaviour, but this has not yet been achieved, due to the enriched uranium alloy proving to be a great deal stronger than information available at the time that the experiments were planned had suggested.† Indeed, the whole experimental programme has been very much a venture into the unknown, with little prior knowledge of material properties and practically none of the problems of measurement in the extremely hostile environment. As far as the elastic dynamic displacements of cylinders and cones are concerned, the authors have succeeded in obtaining good agreement between experimental measurements and the theoretically predicted values: thus publication at this stage seems worthwhile, even though it is hoped in future to improve the experimental techniques and to extend the work to other configurations and to inelastic behaviour.

Section 1 of the paper describes the pulsed reactor, its mode of operation, and the temporal and spatial distributions of temperature to be expected in the experimental specimens.

Section 2 is divided into three parts: the first gives a general analysis of the stresses and displacements and the second and third present detailed results for cylinders and for cones.

Section 3 is also divided into three parts. The first describes the experimental specimens and the temperatures which they experience under neutron heating. The second discusses the mechanical properties of enriched uranium. The third is concerned with the proximity transducers used to measure displacements, and the problems of operation close to a fissile surface.

Section 4 presents the experimental displacements and compares them with the results of the analyses of § 2.

† The strength and ductility of uranium obtained in room temperature tests depend very much on the presence of small quantities of hydrogen—see Adamson, Norman & Picton (1969).

PHILOSOPHICAL TRANSACTIONS OF THE ROYAL SOCIETY A MATHEMATICAL, PHYSICAL & ENGINEERING SCIENCES

Notation

B	$(\omega l/2\pi)\sqrt{(\rho/E)}$
C	r_0/l
d	maximum temperature occurs at $x = d$ (see equation (5))
D	d/l
E	Young modulus
F	total fissions to time t
k	constant in temperature distribution equation (5)
K	kl
l	length of cylinder or cone
m	ur
$\overline{m}$	Laplace transform of m
$[M_U]_{X=1}$	dynamic magnification factor for U at $X = 1$
n	number of term in series
p	parameter in Laplace transform
r	$x+r_0$, coordinate measured from apex of cone
r_0	value of r at which cone is encastred
R_n	roots of equation $(1+C)\,R_n = \tan R_n$ (see table 1)
S	nondimensional stress, $\sigma/E\alpha\theta$
$[S]_{X=0}$	maximum value of S at $X = 0$
t	time from beginning of pulse
t_{m}	time at which rate of fission is a maximum
T	nondimensional time, $\omega t/2\pi$
u	displacement in direction of r
U	nondimensional displacement, $u/\alpha\theta l$
x	coordinate measured from fixed end of cone, in same sense as r
X	nondimensional coordinate, x/l
α	coefficient of linear expansion
α_0	$(\kappa_0-1)/\tau$; reactor period $= 1/\alpha_0$
β	rate of temperature rise
κ_0	prompt reproduction factor at beginning of pulse
λ	temperature rise
μ	temperature coefficient of reactivity
ρ	density
σ	stress
σ_y	yield stress
θ	maximum temperature rise
τ	average neutron lifetime
ω	$\frac{1}{4}\pi\alpha_0$, but see § 4

PHILOSOPHICAL TRANSACTIONS OF THE ROYAL SOCIETY A MATHEMATICAL, PHYSICAL & ENGINEERING SCIENCES

1. The pulsed reactor

The fast pulsed reactor Viper has been described in detail by Weale *et al.* (1968) and by McTaggart *et al.* (1968). It will be convenient, however, to give a brief summary of its mode of operation here for the benefit of those unfamiliar with the device. A simplified diagram of the reactor is shown in figure 1. The fissile parts consist of a fixed central core, two movable safety blocks and a pulse rod which can be inserted rapidly in a hole in the central core. The core and safety blocks contain fuel rods (figure 2) consisting of enriched uranium (37.5 % ^{235}U) alloyed

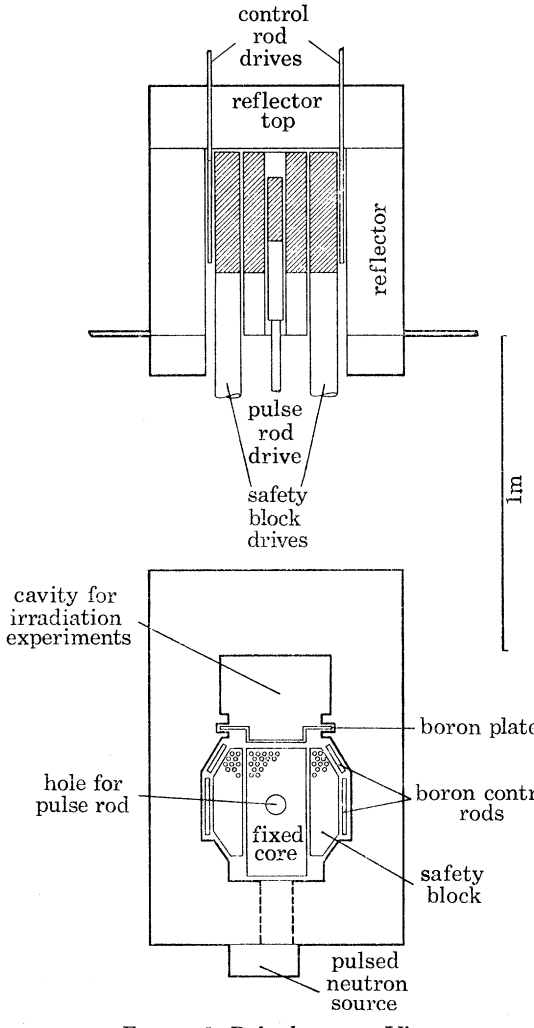

Figure 1. Pulsed reactor Viper.

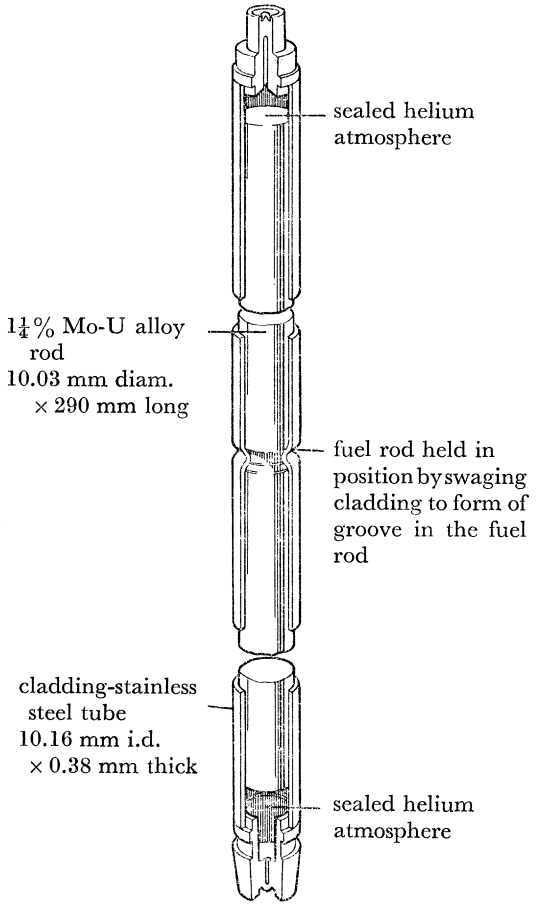

Figure 2. Fuel rod.

with 1.25 % molybdenum. These rods are held at their centres so that sudden heating produces no net force on the core. The pulse rod contains a uranium cylinder of the same composition as the core. The core is surrounded by four movable boron control rods and by a copper reflector. Within the reflector is a space for irradiation experiments: a boron plate separates this space from the core in order to absorb any slow neutrons produced in the experimental specimen. Figure 3, plate 11, is a photograph of the reactor core with the reflector top and core box lid removed and the safety blocks lowered.

In order to understand the mode of operation of Viper it is important to recall that two types

of neutrons are produced in a fission reaction: there are prompt neutrons emitted within 10^{-14} s of fission and delayed neutrons arising from the decay of fission products with half-lives varying from 0.15 s to over 50 s. The delayed neutrons represent only 0.73 % of the total neutron production from ^{235}U fission, but they are extremely important in reactor control. For stable operation, the total rate of production of neutrons (including delayed neutrons) must equal the total rate of absorption. This stable condition, which always obtains in an ordinary power reactor, is known as 'delayed critical'. If the rate of production of prompt neutrons only is equal to the total rate of absorption, the reactor is said to be at 'prompt critical'.

At the beginning of a pulse, Viper is first brought to stable operation at delayed critical and at a very low power. The safety blocks are in and the pulse rod is out. The pulse rod is now rapidly inserted: its mass is such that the reactivity is raised above prompt critical (i.e. more prompt neutrons are being produced than the total number of neutrons absorbed). Such a situation is clearly highly unstable, and the reactor power rises rapidly (although the power would rise naturally, the pulse is in fact triggered by a burst of neutrons from an accelerator source—see figure 1 and Gow & Pollock (1960)). In about 3 ms the power rises to a maximum of 20 GW and the fuel temperature rises by 400 K. The rise in fuel temperature reduces reactivity in two ways. The expansion of the fuel increases the volume of the core and thus lowers reactivity. In addition there is the Doppler effect. A rise of temperature increases both the rate of neutron production in ^{235}U and the rate of neutron absorption in ^{238}U. Which effect predominates depends on the composition of the fuel. In the case of Viper fuel (37.5 % ^{235}U) the Doppler effect lowers reactivity: for a highly enriched fuel it would raise it.

As a result of both the volume increase and the Doppler effect the reactivity is reduced below prompt critical (but still above delayed critical) and the reactor reaches transient equilibrium at a power of about 20 MW. The reactivity must now be reduced below delayed critical as quickly as possible. This is partly because the arrival of delayed neutrons would cause a further increase of power, but also because 20 MW if continued for 0.5 s would double the fuel temperature rise. This further reduction in reactivity is achieved by driving out the safety blocks hydraulically with an acceleration of about 5 g.

The time variation of the neutron pulse, and thence the temperature rise in the fuel rods or specimen, can be determined from the simple reactor model of Wimett (1960). Ignoring delayed neutrons, Wimett's analysis leads to the equation (see Weale *et al.* 1968)

$$\frac{\mathrm{d}^2F}{\mathrm{d}t^2} = \frac{1}{\tau}\frac{\mathrm{d}F}{\mathrm{d}t}[\kappa_0 - 1 - \mu\kappa_0 F], \tag{1}$$

where F denotes the total fissions to time t, κ_0 the prompt reproduction factor at the beginning of the pulse, τ the average neutron lifetime, and μ the temperature coefficient of reactivity. Assuming that heat conduction is negligible in the time interval with which we are concerned, temperature rise λ is proportional to F, provided that the fission fragments are all contained within the fuel and heat from prompt gamma emitters has the same distribution as the ^{235}U fission heating. McTaggart *et al.* (1968) have shown that the fission fragments are contained and in Weale *et al.* (1968) it is found that γ radiation heating accounts for only 7 % of the total heat input, so differences in distribution from the neutron heating are not important.

Provided that one assumes that F and $\mathrm{d}F/\mathrm{d}t$ are negligibly small at the beginning of the pulse, equation (1) can be solved (Hansen 1952) as

$$\lambda = \theta\frac{\exp[\alpha_0(t-t_\mathrm{m})]}{1+\exp[\alpha_0(t-t_\mathrm{m})]}, \tag{2}$$

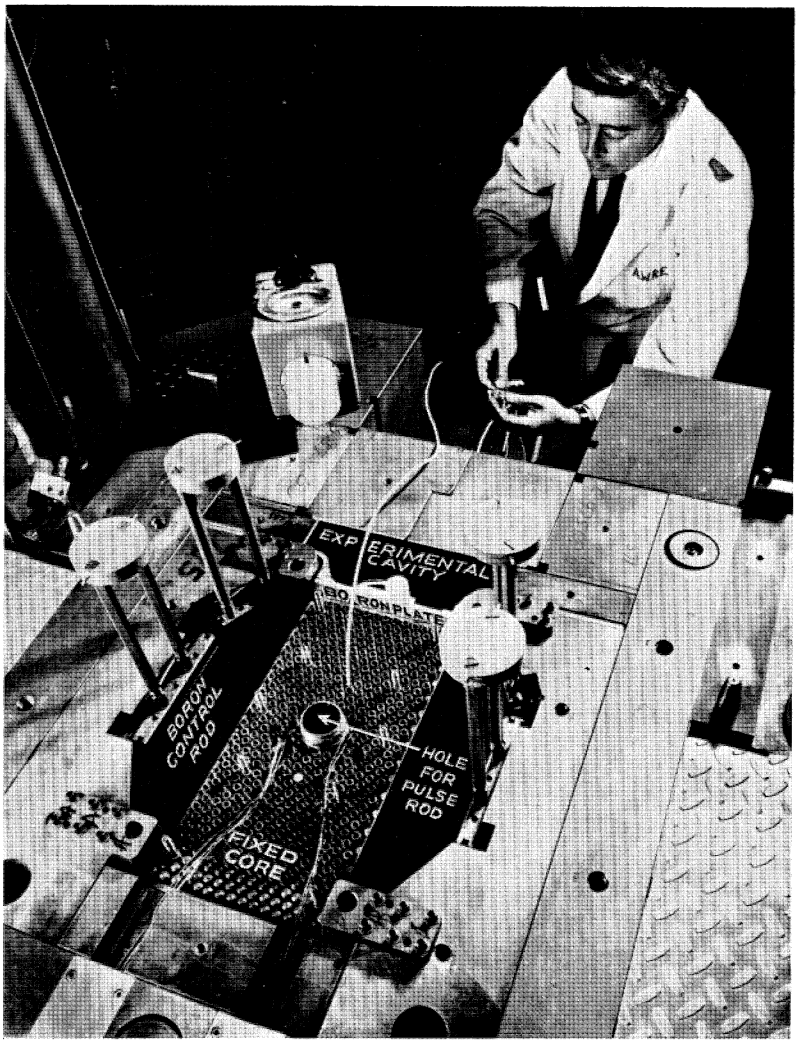

FIGURE 3. Reactor core with reflector top and core box lid removed and the safety blocks lowered.
(U.K.A.E.A. Copyright)

(*Facing p.* 330)

PHILOSOPHICAL TRANSACTIONS OF THE ROYAL SOCIETY A MATHEMATICAL, PHYSICAL & ENGINEERING SCIENCES

where $\alpha_0 = (\kappa_0 - 1)/\tau$, t_m denotes the time at which $\partial F/\partial t$ is a maximum, and θ is the maximum temperature rise.

The temperature–time relation given by equation (2) is not very convenient for analytical work, and so we shall usually replace it by

$$\lambda = \{(\theta/2\pi)\,(\omega t - \sin\omega t) + [\theta - (\theta/2\pi)\,(\omega t - \sin\omega t)]_{\omega t > 2\pi}\}, \tag{3}$$

where

$$\omega = \tfrac{1}{4}\pi\alpha_0, \tag{4}$$

and the term in square brackets is zero for $\omega t < 2\pi$. Equation (4) is obtained by equating the maximum slopes of the functions in equations (2) and (3).

Equations (2) and (3) are plotted non-dimensionally in figure 4. In fact, for Viper, α_0 is about $10^4\,s^{-1}$ and the pulse width at half maximum power is about 0.4 ms.

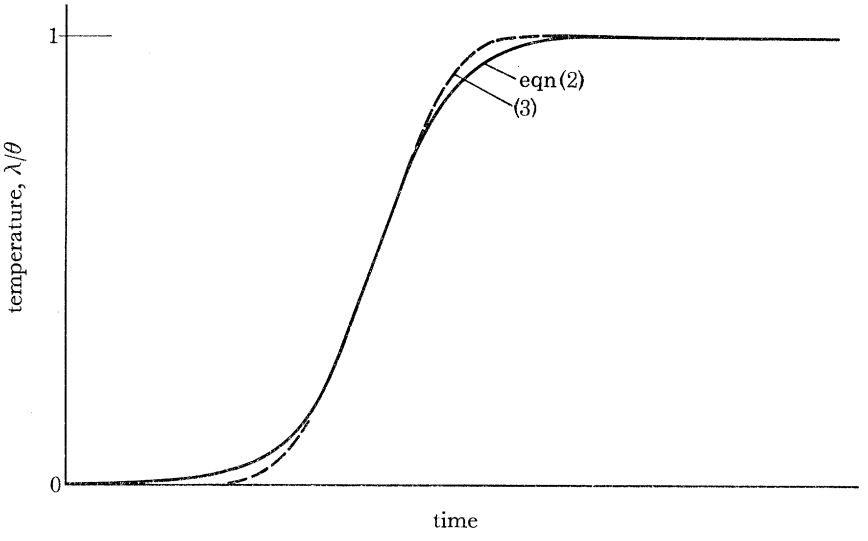

FIGURE 4. Temperature–time relations.

The spatial distribution of temperature rise might be expected from elementary theory (Glasstone & Edlund 1953) to vary sinusoidally along the length of a fuel rod or specimen in the cavity. This was confirmed experimentally by using fission foils or thermocouples, the general form being

$$\lambda = \theta \cos k(x - d), \tag{5}$$

where x is a co-ordinate measured from the fixed end of a specimen and k and d are constants (from symmetry, d is zero for fuel rods).

The maximum temperature attained in a specimen can be changed in three ways; varying the form of the pulse, varying the composition of the fissile material and surrounding the specimen with a polyethylene moderator. The moderator attenuates the neutron energy levels and results in increased capture of neutrons by ^{235}U. There was some initial concern on the part of the authors that self-shielding effects might be important with moderated specimens, i.e. the temperature might vary through the section if the neutron energy levels were low. Tests on a stack of fission foils on the surface of a moderated specimen showed that the self-shielding occurred in a very thin surface layer and that inside that layer the temperature was sensibly constant throughout the cross-section.

2. Stresses and displacements in cylinders and cones

2.1. *General analysis*

As explained in the introduction, the analysis of dynamic thermal stresses in cylinders was developed for fuel rods in 1965 and was later extended to cones when it was decided to use conical experimental specimens to increase stress levels and in the hope of inducing plasticity. It will be briefer for our present purposes if we give the analysis for cones first, and treat cylinders as cones of zero taper. The analysis is one-dimensional. Experimental work by Kenner & Goldsmith (1968) has suggested that one-dimensional theory is satisfactory for cones of up to 5° apex angle: those used in our experiments had an apex angle of 1.48°. An analysis of radial effects by perturbation techniques is given by Rogge (1970).

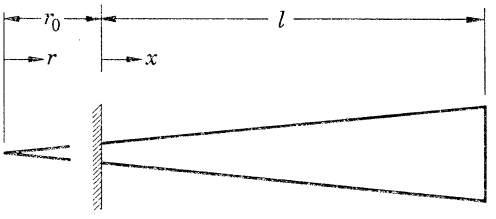

Figure 5. Cone.

Consider a slender truncated cone (figure 5) encastred at $r = r_0$, where r is a coordinate measured from the apex. Let x be a coordinate measured along the cone from the fixed end, in the same sense as r, so that

$$r = x + r_0. \tag{6}$$

Let the free end of the cone be at $x = l$. Then if l is positive the cone is held at its smaller end, and if l is negative the cone is held at its larger end.

If the displacement of any section of the cone in the direction of r is u and the stress at that section is σ, we have the constitutive equation

$$\frac{\partial u}{\partial r} = \frac{\sigma}{E} + \alpha\lambda, \tag{7}$$

where E is the Young modulus and α the coefficient of linear expansion.

The equation of motion of an element of the cone is

$$\frac{\partial(\sigma r^2)}{\partial r} = \rho r^2 \frac{\partial^2 u}{\partial t^2}, \tag{8}$$

where ρ is the density.

Eliminating σ between (7) and (8) and substituting from (6) we have

$$\frac{\partial^2 m}{\partial t^2} - \frac{E}{\rho}\frac{\partial^2 m}{\partial x^2} = -\frac{E\alpha}{\rho}\left\{(x + r_0)\frac{\partial \lambda}{\partial x} + 2\lambda\right\}, \tag{9}$$

where

$$m = ur. \tag{10}$$

Equation (9), with the right-hand side equal to zero, was used by Landon & Quinney (1923) in some of the earliest experimental work on stress waves in a conical bar. They solved it in terms of wave propagation ($m = f(x \pm (E/\rho)^{\frac{1}{2}}t)$): it is more convenient for us to proceed differently.

Equation (9) has to be solved subject to a number of initial and boundary conditions and to a particular temperature history. Assuming that the cone is initially at datum temperature and at rest we have:

$$\left.\begin{aligned} &m = \partial m/\partial t = 0 \quad \text{at} \quad t = 0 \quad \text{for} \quad 0 \leqslant x \leqslant l, \\ &m = 0 \quad \text{at} \quad x = 0 \quad \text{for all } t, \\ &\sigma = 0 \quad \text{at} \quad x = l \quad \text{and thus} \quad \partial m/\partial x = m/(x+r_0) + (x+r_0)\,\alpha\lambda \\ &\qquad\qquad\qquad\qquad\qquad\qquad\qquad\qquad \text{at} \quad x = l \quad \text{for all } t. \end{aligned}\right\} \tag{11}$$

Combining (3) and (5):

$$\lambda = \{(\theta/2\pi)\,(\omega t - \sin\omega t) + [\theta - (\theta/2\pi)\,(\omega t - \sin\omega t)]_{\omega t > 2\pi}\}\cos k(x-d) \quad \text{for} \quad t \geqslant 0.$$

Applying the single-sided Laplace transform

$$\bar{f}(x) = \int_0^\infty \mathrm{e}^{-pt} f(x,t)\,\mathrm{d}t$$

to equation (9) and using the initial conditions and temperature distribution of (11) we have

$$p^2\bar{m} - \frac{E}{\rho}\frac{\mathrm{d}^2\bar{m}}{\mathrm{d}x^2} = \frac{E\alpha\theta}{2\pi\rho}\{k(x+r_0)\sin k(x-d) - 2\cos k(x-d)\} \times\left\{\frac{\omega^3}{p^2(\omega^2+p^2)} - \left[\frac{\omega^3\,\mathrm{e}^{-2\pi p/\omega}}{p^2(\omega^2+p^2)}\right]\right\}, \tag{12}$$

with transformed boundary conditions

$$\left.\begin{aligned} &\bar{m} = 0 \quad \text{at} \quad x = 0, \\ &\frac{\mathrm{d}\bar{m}}{\mathrm{d}x} = \frac{\bar{m}}{l+r_0} + \frac{\alpha\theta(l+r_0)\cos k(l-d)}{2\pi}\left\{\frac{\omega^3}{p^2(\omega^2+p^2)} - \left[\frac{\omega^3\,\mathrm{e}^{-2\pi p/\omega}}{p^2(\omega^2+p^2)}\right]\right\} \quad \text{at} \quad x = l. \end{aligned}\right\} \tag{13}$$

The solution of equation (12) with boundary conditions (13) is

$$\begin{aligned} \bar{m} = \frac{\alpha\theta}{2\pi(p^2\rho/E+k^2)}\Bigg[&\frac{(l+r_0)\,p(\rho/E)^{\frac{1}{2}}\cos k(l-d) - r_0 k\sin kd\sinh\{p(\rho/E)^{\frac{1}{2}}l\}}{\cosh\{p(\rho/E)^{\frac{1}{2}}l\}}\sinh\{p(\rho/E)^{\frac{1}{2}}x\} \\ &+ (x+r_0)\,k\sin k(x-d) + r_0 k\sin kd\cosh\{p(\rho/E)^{\frac{1}{2}}x\} \\ &+ \frac{2p^2\rho/E}{(p^2\rho/E+k^2)}(\cos kd\cosh\{p(\rho/E)^{\frac{1}{2}}x\} - \cos k(x-d)) \\ &+ \Bigg\{[(l+r_0)\,p(\rho/E)^{\frac{1}{2}}\cos k(l-d) - r_0 k\sin kd\sinh\{p(\rho/E)^{\frac{1}{2}}l\}]\tanh\{p(\rho/E)^{\frac{1}{2}}l\} \\ &+ \frac{2p^2\rho/E}{(p^2\rho/E+k^2)}\Bigg[\left(\cos kd + \tfrac{1}{2}r_0\frac{k(p^2\rho/E+k^2)}{p^2\rho/E}\sin kd\right)\cosh\{p(\rho/E)^{\frac{1}{2}}l\} \\ &- \cos k(l-d) - (l+r_0)\,(p(\rho/E)^{\frac{1}{2}}\cos kd\sinh\{p(\rho/E)^{\frac{1}{2}}l\} + k\sin k(l-d))\Bigg]\Bigg\} \\ &\times\frac{\sinh p(\rho/E)^{\frac{1}{2}}x}{(l+r_0)\,p(\rho/E)^{\frac{1}{2}}\cosh p(\rho/E)^{\frac{1}{2}}l - \sinh p(\rho/E)^{\frac{1}{2}}l}\Bigg]\left\{\frac{\omega^3}{p^2(\omega^2+p^2)} - \left[\frac{\omega^3\,\mathrm{e}^{-2\pi p/\omega}}{p^2(\omega^2+p^2)}\right]\right\}. \end{aligned} \tag{14}$$

Equation (14) can be inverted by contour integration. There is a double pole at $p = 0$ and poles at $p = \pm\mathrm{i}\omega$ and at the roots of

$$(1+C)\,R_n = \tan R_n, \tag{15}$$

where

$$\pm\mathrm{i}R_n = p(\rho/E)^{\frac{1}{2}}l \quad \text{and} \quad C = r_0/l \tag{16}$$

and R_n is positive and real. It should be noted that there are no poles at $p = \pm ik(E/\rho)^{\frac{1}{2}}$ or at $p = \pm \frac{1}{2}in\pi E/l\rho$ for n odd.

The roots of equation (15) are given in table 1 for $C = 0.25, 0.5, 1, \pm\infty, -5, -2$. Successive roots are denoted by odd values of n since for the cylinder ($C = \pm\infty$) the solution of equation (15) is $R_n = \frac{1}{2}n\pi$ (n odd), and, for all values of C except -1, R_n tends to $\frac{1}{2}n\pi$ as n becomes large (for $C = -1$, the values of R_n are $\frac{1}{2}(n+1)\pi$).

TABLE 1. ROOTS OF $(1+C)R_n = \tan R_n$

n	$C = 0.25$	$C = 0.50$	$C = 1.00$	$C = \pm\infty$	$C = -5.00$	$C = -2.00$
1	0.7593	0.9674	1.1656	1.5708	1.7155	2.0288
3	4.5379	4.5675	4.6042	4.7124	4.7648	4.9132
5	7.7511	7.7684	7.7899	7.8540	7.8857	7.9787
7	10.9225	10.9347	10.9499	10.9956	11.0183	11.0855
9	14.0804	14.0899	14.1017	14.1372	14.1548	14.2074
11	17.2324	17.2401	17.2498	17.2788	17.2932	17.3364
13	20.3811	20.3877	20.3958	20.4203	20.4326	20.4692
15	23.5279	23.5336	23.5407	23.5619	23.5725	23.6043
17	26.6735	26.6785	26.6848	26.7035	26.7129	26.7409
19	29.8183	29.8228	29.8284	29.8451	29.8535	29.8786
21	32.9624	32.9665	32.9715	32.9867	32.9943	33.0170
23	36.1061	36.1098	36.1144	36.1283	36.1352	36.1559
25	39.2495	39.2529	39.2571	39.2699	39.2762	39.2953
large			all values tend to $\frac{1}{2}n\pi$			

On inversion, equation (15) becomes

$$
\begin{aligned}
U = {} & \frac{\sin K(X-D)+\sin KD}{K}\{T-[T-1]_{T>1}\} \\
& + \frac{\sin 2\pi T}{2\pi(K^2-4\pi^2B^2)}\left[K\sin K(X-D)+\frac{C}{C+X}K\sin KD\cos 2\pi BX\right. \\
& - \frac{(C+1)\,2\pi B\cos K(1-D)-C\sin KD\sin 2\pi B}{(C+X)\cos 2\pi B}\sin 2\pi BX - \frac{8\pi^2B^2}{K^2-4\pi^2B^2} \\
& \times \frac{(\cos KD\cos 2\pi BX-\cos K(X-D))}{C+X} \\
& - \left\{((C+1)\,2\pi B\cos K(1-D)-CK\sin KD\sin 2\pi B)\tan 2\pi B+\frac{8\pi^2B^2}{K^2-4\pi^2B^2}\right. \\
& \times \left[\left(\cos KD-\frac{CK(K^2-4\pi^2B^2)}{8\pi^2B^2}\sin KD\right)\cos 2\pi B-\cos K(1-D)\right. \\
& \left.\left.-(C+1)\,(K\sin K(1-D)-2\pi B\cos KD\sin 2\pi B)\right]\right\} \\
& \left.\times\frac{\sin 2\pi BX}{(C+X)\{(C+1)\,2\pi B\cos 2\pi B-\sin 2\pi B\}}\right]\{-1+[1]_{T>1}\} \\
& + \sum_{n=1,\,3,\,5\ \text{etc.}} \frac{8\pi^2B^3\sin R_nX}{(R_n^2-K^2)\,(R_n^2-4\pi^2B^2)}\left[\frac{\left\{(C+1)^2\cos K(1-D)-(C+1)\frac{K}{R_n}\sin KD\sin R_n\right.\right. \\
& \left.\left.+\frac{2}{R_n^2-K^2}\left[(C+1)\,(K\sin K(1-D)\right.\right.\right. \\
& \left.\left.\left.-R_n\cos KD\sin R_n)-\left(\cos KD+\frac{CK(R_n^2-K^2)}{2R_n^2}\right.\right.\right. \\
& \left.\left.\left.\times\sin KD\right)\cos R_n+\cos K(1-D)\right]\right\}}{(C+X)\{(C+1)\,R_n\sin R_n-C\cos R_n\}}\right] \\
& \times\left\{\sin R_n\frac{T}{B}-\left[\sin R_n\frac{(T-1)}{B}\right]_{T>1}\right\}, \qquad (17)
\end{aligned}
$$

where we have introduced the non-dimensional parameters

$$\left.\begin{aligned} U &= u/\alpha\theta l, & T &= \omega t/2\pi, \\ X &= x/l, & K &= kl, \\ D &= d/l, & B &= (\omega l/2\pi)\,(\rho/E)^{\frac{1}{2}}. \end{aligned}\right\} \tag{18}$$

It will be seen that U is the displacement as a fraction of that which would occur at $X = 1$ if the whole cone were subjected to the maximum temperature rise, T is a nondimensional time such that the pulse ends at $T = 1$, and B is the ratio of the time taken for an elastic wave to travel the length of the rod to the period of the pulse.

Once U is known the stresses can be obtained from equation (7). A convenient nondimensional form is

$$S = \frac{\sigma}{E\alpha\theta} = \frac{\partial U}{\partial X} - \frac{\lambda}{\theta}, \tag{19}$$

where S is the stress expressed as a fraction of that which would occur if all longitudinal displacement were prevented and the cone was heated to a uniform temperature θ.

2.2. *The cylinder*

For $C = \pm\infty$, equation (17) takes the simpler form

$$\begin{aligned} U = {} & \frac{\sin K(X-D)+\sin KD}{K}\{T-[T-1]_{T>1}\}+\frac{\sin 2\pi T}{2\pi(K^2-4\pi^2B^2)\cos 2\pi B} \\ & \times[K\cos 2\pi B(\sin K(X-D)+\sin KD\cos 2\pi BX) \\ & -\sin 2\pi BX(2\pi B\cos K(1-D)-K\sin KD\sin 2\pi B)]\{-1+[1]_{T>1}\} \\ & +\sum_{n=1,3\ 5,\ldots}\frac{8\pi^2B^3(\cos K(1-D)-(2K/n\pi)\sin KD\sin\frac{1}{2}n\pi}{\frac{1}{2}n\pi\,(\frac{1}{4}n^2\pi^2-K^2)\,(\frac{1}{4}n^2\pi^2-4\pi^2B^2)}\frac{\sin\frac{1}{2}n\pi X}{\sin\frac{1}{2}n\pi} \\ & \times\left\{\sin\frac{n\pi T}{2B}-\left[\sin\frac{n\pi}{2B}(T-1)\right]_{T>1}\right\}. \end{aligned} \tag{20}$$

After the heating pulse has ended ($T > 1$) the second term in equation (20) is zero. The first term represents the expansion which would occur if the pin were heated slowly. The third term represents a residual oscillation of the rod. For $T > 1$, equation (20) can be written as

$$\begin{aligned} U = {} & \frac{\sin K(X-D)+\sin KD}{K}+\sum_{n=1,3,5,\ldots}\frac{16\pi^2B^3\,(\cos K(1-D)-(2K/n\pi)\sin KD\sin\frac{1}{2}n\pi)}{\frac{1}{2}n\pi(\frac{1}{4}n^2\pi^2-K^2)\,(\frac{1}{4}n^2\pi^2-4\pi^2B^2)} \\ & \times\frac{\sin\frac{1}{2}n\pi X}{\sin\frac{1}{2}n\pi}\sin\frac{n\pi}{4B}\cos\frac{n\pi}{4B}(2T-1). \end{aligned} \tag{21}$$

For small values of B it is clear that the first term in the series ($n = 1$) predominates, so that the oscillation is almost purely sinusoidal: it can be imagined as beginning (with maximum negative amplitude) at $T = \frac{1}{2}$ with a period of $T = 4B$ or $t = 4l(\rho/E)^{\frac{1}{2}}$.

Further simplification is possible by restricting our attention to the case $D = 0$. This represents the symmetrical heating of a cylinder held at its centre, and corresponds to a Viper fuel rod. The maximum value of U occurs at $X = 1$ and if we take the ratio of this maximum displacement to that which would occur with slow heating ($\sin K/K$) we get the dynamic magnification factor for U,

$$[M_U]_{X=1} = 1+\left|\sum_{n=1,3,5\ldots}\frac{16\pi^2B^3K\cot K}{\frac{1}{2}n\pi(\frac{1}{4}n^2\pi^2-K^2)\,(\frac{1}{4}n^2\pi^2-4\pi^2B^2)}\sin\frac{n\pi}{4B}\right|. \tag{22}$$

The stress oscillates in phase with U. The amplitude at the fixed end of the cylinder is given by

$$[S]_{X=0} = \left| \sum_{n=1,\,3,\,5\,\ldots} \frac{16\pi^2 B^3 \cos K}{(\frac{1}{4}n^2\pi^2 - K^2)\,(\frac{1}{4}n^2\pi^2 - 4\pi^2 B^2)} \frac{\sin\,(n\pi/4B)}{\sin\,\frac{1}{2}n\pi} \right|. \tag{23}$$

The values of $[M_U]_{X=1}$ and $[S]_{X=0}$ are plotted in figure 6 for $\cos K = 0$, 0.5 and 1 and for $B = 0$ to 2. It will be seen that the dynamic effects become almost fully operative for values of B in excess of 0.5. With the present Viper core, the maximum attainable value of B in the core fuel rods is about 0.05 and in a longer cylindrical rod in the experimental cavity is about 0.1, so that dynamic effects in the core are negligible and even in the cavity are very small. A point of some interest is that there is no oscillation after $T = 1$ when $B = \frac{1}{8}, \frac{1}{12}, \frac{1}{16}, \frac{1}{20}, \ldots$.

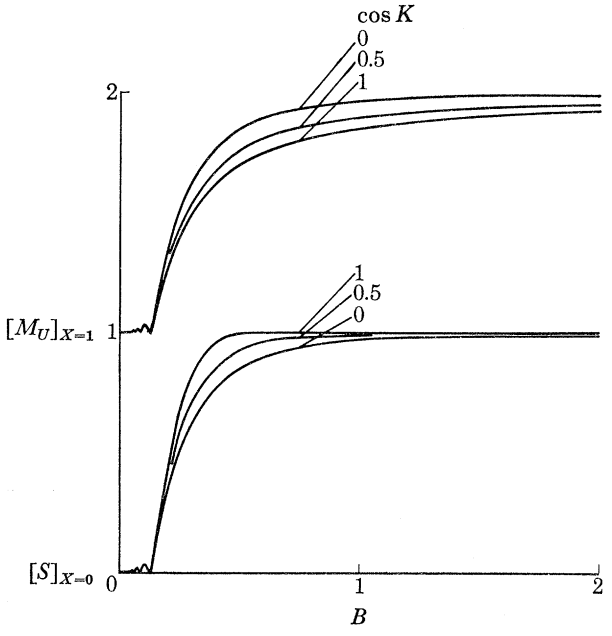

FIGURE 6. Variation of $[M_U]_{X=1}$ and $[S]_{X=0}$ for a cylinder with B.

A more detailed picture of the displacements and stresses in a cylinder encastré at one end is given in figures 7 to 9. Figure 7 (*a*) shows the displacement of the free end as a function of time for $D = 0$, $\cos K = 0.5$, and for various values of B. The almost purely sinusoidal oscillation about the mean position for values of B up to about 0.5 can be clearly seen. Figure 7 (*b*) shows a similar plot, but on an extended time scale, for $\cos K = 1$. It will be noticed that for $B = 1$ and 2 the oscillation is tending towards a triangular form: this is to be expected since if B is large, equation (21) becomes for $D = 0$ and $X = 1$

$$[U]_{X=1} = 1 - \sum_{n=1,\,3,\,5\,\ldots} \frac{8}{n^2\pi^2} \cos\frac{n\pi}{4B}\,(2T-1), \tag{24}$$

which is the equation of a triangular wave.

Figure 8 shows the stress at the fixed end of the cylinder for $\cos K = 0.5$ and 1 and various values of B. Here again the oscillation is sinusoidal for $B \leqslant 1$, but for $B = 2$ the pattern is tending towards a square wave. If we calculate the stress from equations (19) and (21) and put $K = D = X = 0$, we have for B large

$$[S]_{X=0} = -\sum_{n=1,\,3,\,5\,\ldots} \frac{4}{n\pi} \sin\tfrac{1}{2}n\pi \cos\frac{n\pi}{4B}\,(2T-1), \tag{25}$$

which is the equation of a square wave.

Figure 9 shows the variation of stress with time for $\cos K = 1$, $B = 2$ and $X = 0\,(0.1)\,1$. An important point to notice here is that the maximum stress does not necessarily occur at $X = 0$.

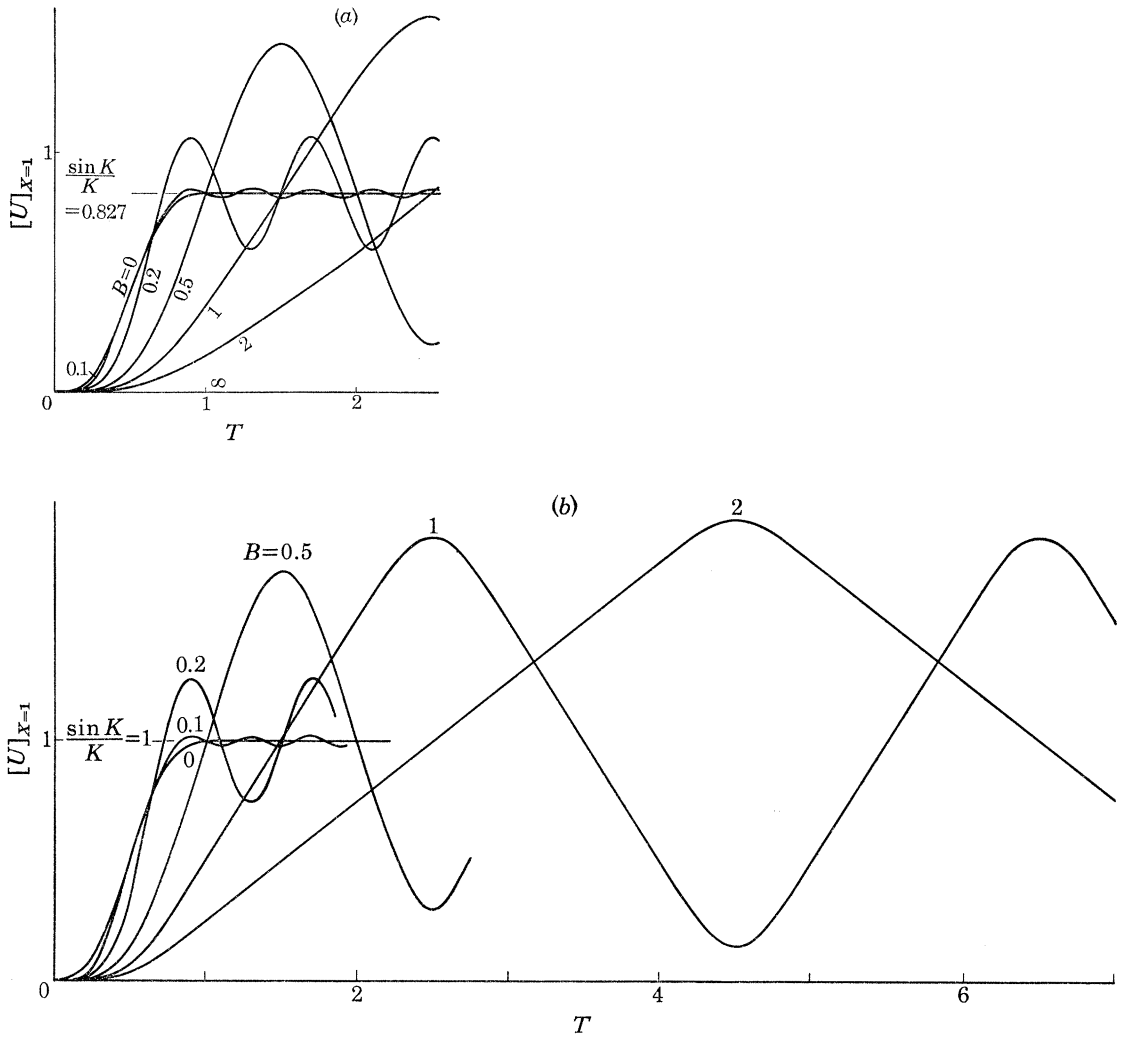

FIGURE 7. (*a*) End displacement of cylinder, $D = 0$, $\cos K = 0.5$; (*b*) End displacement of cylinder, $D = 0$, $\cos K = 1$.

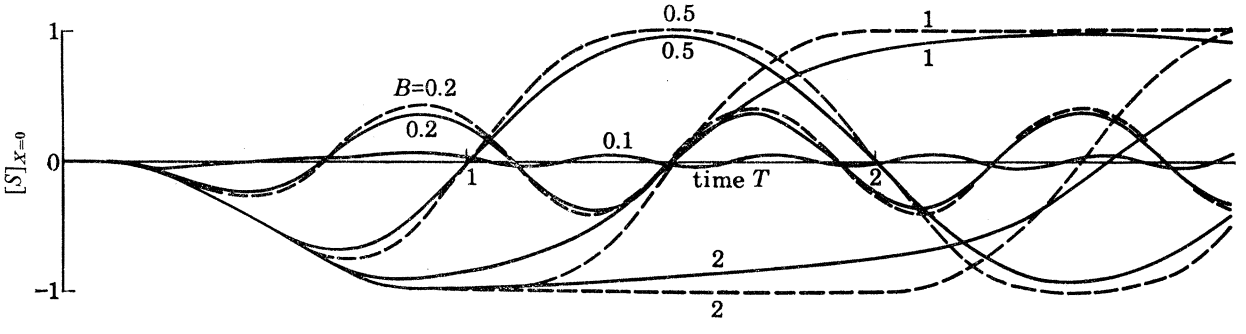

FIGURE 8. Root stress in a cylinder. ———, $\cos K = 1$; ——, $\cos K = 0.5$.

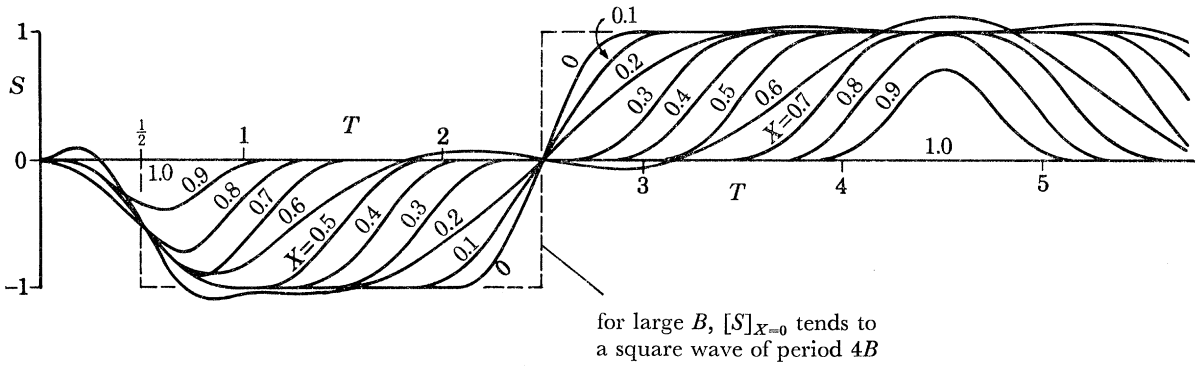

FIGURE 9. Stresses in a cylinder for $\cos K = 1$, $B = 2$.

2.3. *The cone*

For $T > 1$ equation (17) can be written as

$$U = \frac{\sin K(X-D) + \sin KD}{K} + \sum_{n=1,3,5\ldots} \frac{16\pi^2 B^3 \sin R_n X}{(R_n^2 - K^2)(R_n^2 - 4\pi^2 B^2)} \left[\frac{\left\{ (C+1)^2 \cos K(1-D) - (C+1)\frac{K}{R_n} \sin KD \sin R_n + \frac{2}{R_n^2 - K^2}\left[(C+1)(K \sin K(1-D) - R_n \cos KD \sin R_n) - \left(\cos KD + \frac{CK(R_n^2 - K^2)}{2R_n^2} \times \sin KD \right) \cos R_n + \cos K(1-D) \right] \right\}}{(C+X)\{(C+1) R_n \sin R_n - C \cos R_n\}} \right] \times \sin \frac{R_n}{2B} \cos \frac{R_n}{2B} (2T-1). \quad (26)$$

This is similar in form to equation (21) and again the first term represents the expansion under slow heating and the second an oscillation in which for small values of B the first term in the series predominates. The oscillation can again be imagined as beginning with maximum negative amplitude at $T = \frac{1}{2}$ and the period is $T = 2\pi B/R_1$ or $t = 2\pi l(\rho/E)^{\frac{1}{2}}/R_1$.

Figure 10 shows the variation of the dispacement of the free end of the cone with time for a particular set of parameters $B = 0.2$, $D = 0$, $\cos K = 0.5$ and for various values of C. The almost purely sinusoidal form of the oscillation can be seen, and also the way in which the dynamic magnification factor varies with cone geometry, reaching a maximum for cones having small positive values of C. Figure 11 shows the variation of the root stress with time, for the same set of parameters. As would be expected, the maximum stress in a cone always occurs at the root when C is small positive. As we have already seen, this is not true when C becomes large (cylinders) or negative. Figure 12 shows the dynamic magnification factor on end displacement $[M_U]_{X=1}$ and the root stress $[S]_{X=0}$ as functions of C for $D = 0$ and $\cos K = 0.5$ and for $B = 0.1$ and 0.2. It will be seen that changing from a cylindrical form ($C = \pm\infty$) to a cone held at its smaller end (C positive finite) can produce large root stresses even for these comparatively small values of B. The dynamic magnification factor on end displacement, however, is relatively insensitive to changes in geometry.

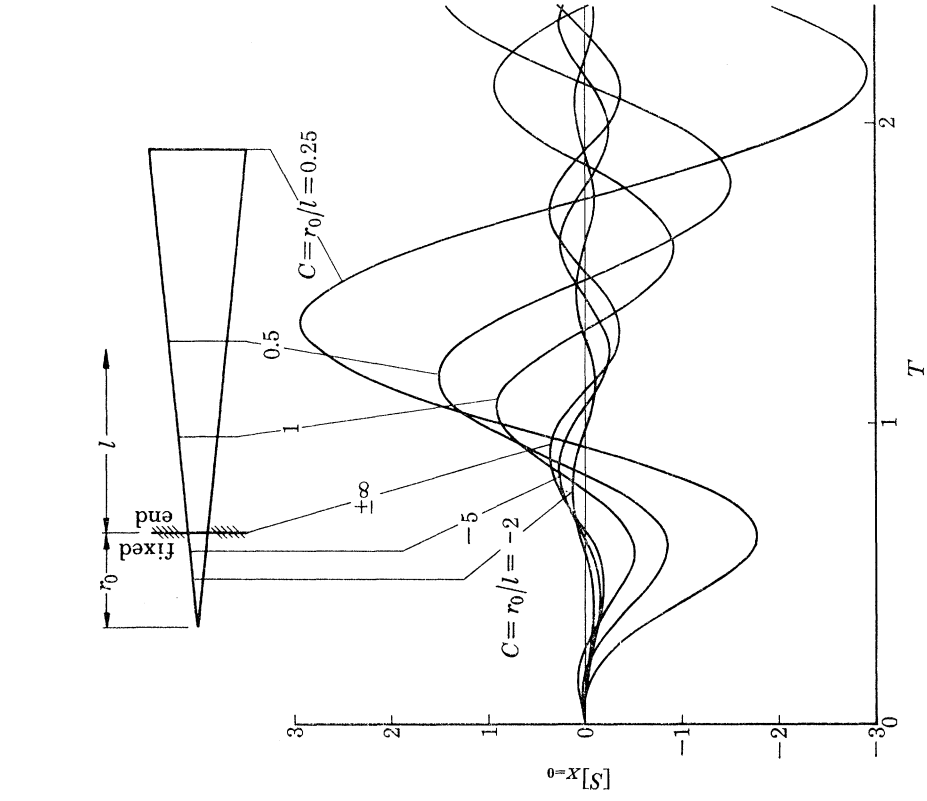

FIGURE 11. Root stress in a cone. $D = 0$; $\cos K = 0.5$; $B = 0.2$.

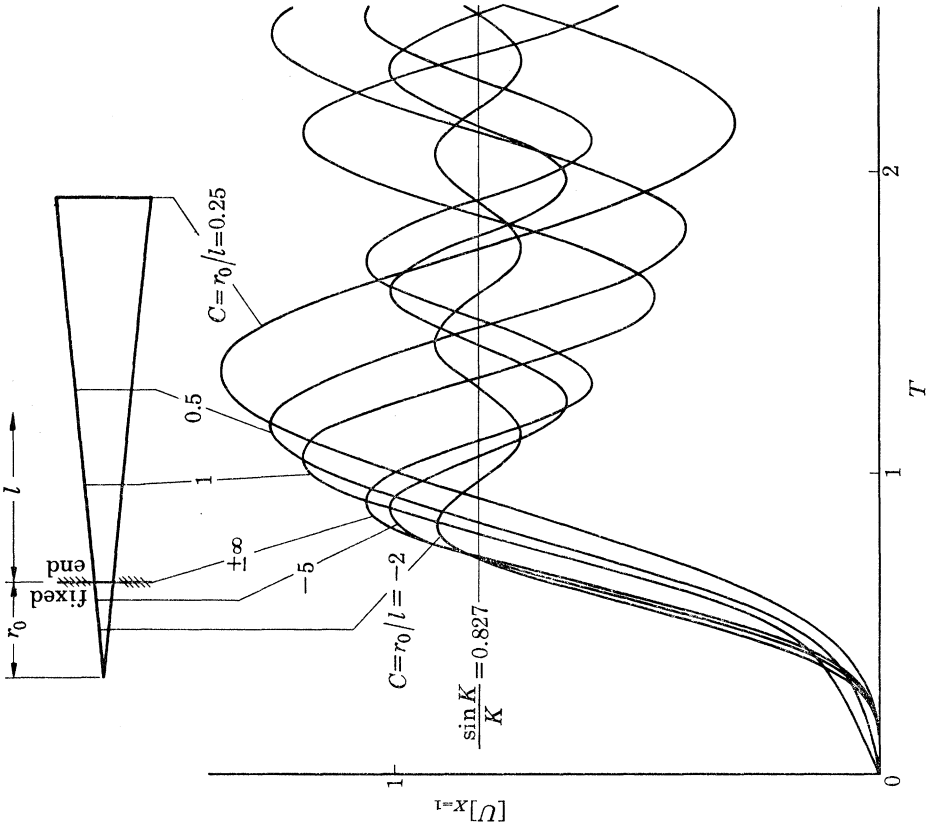

FIGURE 10. End displacement of a cone. $D = 0$; $\cos K = 0.5$; $B = 0.2$.

PHILOSOPHICAL TRANSACTIONS OF THE ROYAL SOCIETY A MATHEMATICAL, PHYSICAL & ENGINEERING SCIENCES

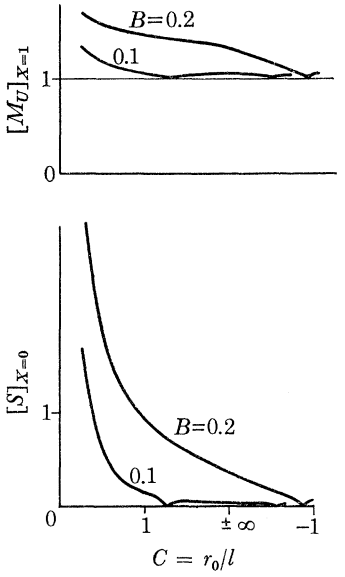

FIGURE 12. Variation of $[M_U]_{X=1}$ and $[S]_{X=0}$ with cone geometry, for $D = 0$ and $\cos K = 0.5$.

3. EXPERIMENTAL WORK

3.1. *Experimental specimens and temperature distributions*

Five different uranium specimens were tested under heating pulses. The first was an ordinary fuel rod of 37.5 % ^{235}U enrichment in the fixed core of the Viper reactor (see figures 1 and 2). The second was a cylinder held at its end in the cavity of the Viper reactor, and having 46 % ^{235}U enrichment. The third specimen was similar to the second, except that it was surrounded by a sleeve of polyethylene moderator. The fourth specimen was a cone held at its smaller end in the experimental cavity, also of 46 % ^{235}U enrichment, and the fifth was similar to the fourth with the addition of a sleeve of moderator. Dimensions of the specimens are given in table 2.

TABLE 2. EXPERIMENTAL SPECIMENS

no.	position	% ^{235}U	length from support mm	max. diam. mm	min. diam. mm	thickness of moderator sleeve mm
1	core	37.5	145	10.0	10.0	—
2	cavity	46	264	7.1	7.1	—
3	cavity	46	264	7.1	7.1	6.7
4	cavity	46	264	10.0	3.2	—
5	cavity	46	264	10.0	3.2	6.7

The axial distribution of temperature along the specimens during heating was measured by using fission foils or thermocouples. It was checked that heat conduction both axially and to any cladding (see figure 2) was negligible during a pulse and that the temperature was proportional to the integrated fission count (see § 1). Figure 13 shows the results for specimens 1 and 2: the appropriate forms of equation (5) are given on the diagrams. Tests on specimen 3 showed general agreement with those on specimen 2, although there was more scatter and some low readings very near to the fixed end, believed to be due to end effects in the moderator sleeve: the same

form of equation (5) will be taken as appropriate. No tests were made on specimens 4 and 5, but since self shielding is known to be small (see § 1) the distribution found for specimen 2 was also thought to be appropriate for them.

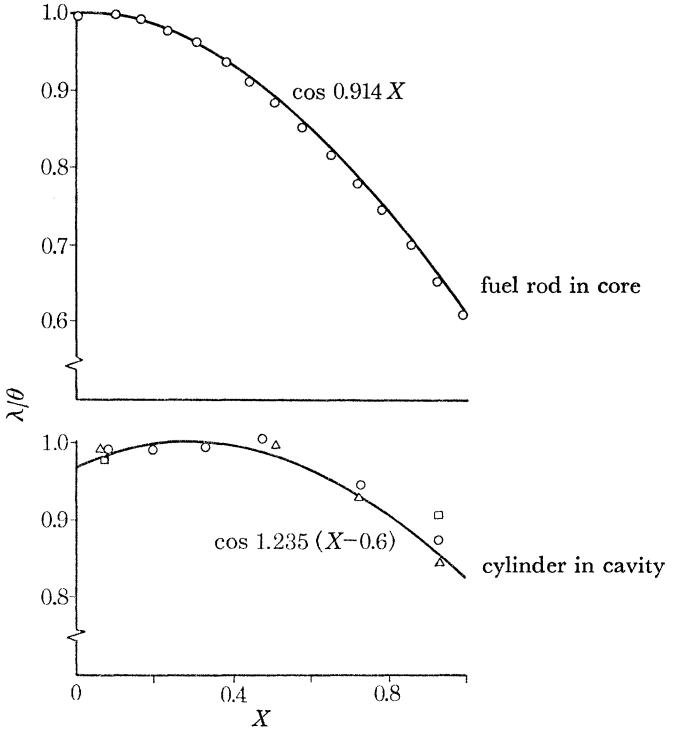

FIGURE 13. Spatial distribution of temperature: ○, fission foils; □, fission foils in lee of specimen; △, thermocouples.

It was not convenient to take temperature measurements on the specimens during the pulses in which displacement measurements were made (see § 3.3), mainly because of limited clearances, and so the maximum temperature in a specimen was related to the reading of a master thermocouple (known as ET 10) in the core of the reactor. It is shown in Weale *et al.* (1968) that the maximum fuel rod temperature rise is 2.00 times the temperature rise measured by ET 10. For specimens in the cavity we found from our thermocouple measurements that the corresponding ratios were 0.88 and 1.80 (moderated).

Another means of checking the accuracy of these ratios is to note the increase in length of a specimen due to heating (see § 3.3). Tests during twenty-three pulses, in which the increase in length was both calculated from the ET 10 reading, using the above ratios of maximum temperature and temperature distributions, and also measured directly showed that for all positions and kinds of specimens the agreement was very close (average values in almost exact agreement, with standard deviation of 5 %).

3.2. *Material properties*

Almost all mechanical testing of uranium and uranium alloys has been done on depleted material, that is uranium containing its natural proportion of ^{235}U (about 0.7 %) which can be handled without the extensive safety precautions necessarily associated with enriched material. However it is known that there is a difference in mechanical properties between the enriched and depleted material, probably due to different methods of manufacture. The authors therefore

decided to carry out tensile tests on fuel rod material (37.5 % ^{235}U) to determine the Young modulus and the ultimate tensile strength at room temperature and at 300 °C (no spare 46 % ^{235}U material could be obtained).

Enough 37.5 % fissile material was available for the manufacture of five specimens of 6.35 mm diameter and 38 mm long between the shoulders. Three were used for room temperature tests and two for tests at 300 °C. The exposed parts of the Instron testing machine were sheathed in polythene. The thermal environment chamber had a disposable steel liner to contain radiation and a flow of argon was maintained through it. Specimens had to be handled with gloves and tended to acquire a loose powdery coating of oxide: they were weighed before and after testing to check loss of radioactive material. Strain measurements were made at room temperature with an extensometer but at elevated temperature less accurately by observing crosshead movement. Strain rates were low (less than 0.25 s^{-1}).

TABLE 3. PROPERTIES OF ENRICHED URANIUM

temperature/°C	Young modulus/GN m^{-2}	u.t.s./GN m^{-2}
15	154	0.89
300	121	0.63

The results of the authors' tensile tests are shown in table 3. The values of the Young modulus are at the lower limit of those commonly quoted for depleted uranium. Gittus (1963) gives values from 145 to 210 GN/m^2 at room temperature with a reduction factor of 0.85 at 300 °C.

The density of uranium at room temperature is 19 070 kg/m^3. Its linear coefficient of expansion varies with temperature. According to McIntosh & Heal (1958) its mean value in the range 0 to 200 °C is 15.3×10^{-6}/K.

3.3. *Measuring apparatus*

The analysis of § 2 was concerned with the dynamic stresses and displacements in cylinders and cones subjected to neutron pulses, and ideally to confirm our theories we should like to measure both of these. The authors' attempts to use electrical resistance strain gauges on the fissile specimens have so far, however, been entirely unsuccessful. The major problem is lack of adhesion due to the formation of an oxide layer on the surface of the uranium, together with the usual contamination hazards with radioactive material. Attention has therefore been concentrated on measuring the displacement of the free end of the specimen (the fact that in all specimens the fissile material had to be placed inside a protective steel can (see figure 2) made displacement measurements at intermediate points impracticable).

The displacement probe used was the reluctance type proximity transducer manufactured by the Bentley Nevada Corporation. The coaxial cables were insulated with radiation-resistant polytetrafluorethylene. Each probe is supplied with its own driver unit consisting of a f.m. oscillator of 1 MHz carrier frequency.

The probes were used in three different ways. First, a probe was attached to the lid of the steel box containing the fixed core. This lid can be regarded as stationary within the time scale of a pulse, and the probe was used to check that the steel can surrounding a specimen did not expand significantly during this period. The steel can was extended by a copper cap silver-plated and then gold flash-plated to inhibit oxide formation, as shown in figure 14 (*a*). Secondly, a probe screwed into the end of the steel can, which could now be regarded as fixed, was used to determine the movement of the end of the specimen (figure 14 (*b*)). Thirdly, near to the specimen, a probe

was screwed into the end of an empty can, 'looking at' a stationary ^{235}U foil, as shown in figure 14 (*c*). This third probe was necessary to measure interference during the pulse. Interference with the probe reading occurs partly because of the intense neutron and gamma radiation passing through the transducer windings, but mostly because if the probe is viewing a surface of fissile material, a layer of ionized gas occurs during a pulse which appears as a false surface to the probe. Tests on non-fissile materials show smaller interference, and the authors did consider trying to bond a shielding layer to the free end of each specimen. The high stress and temperature levels, coupled with the ease with which uranium corrodes, make bonding difficult, however and it was decided instead to compensate for the full fissile interference.

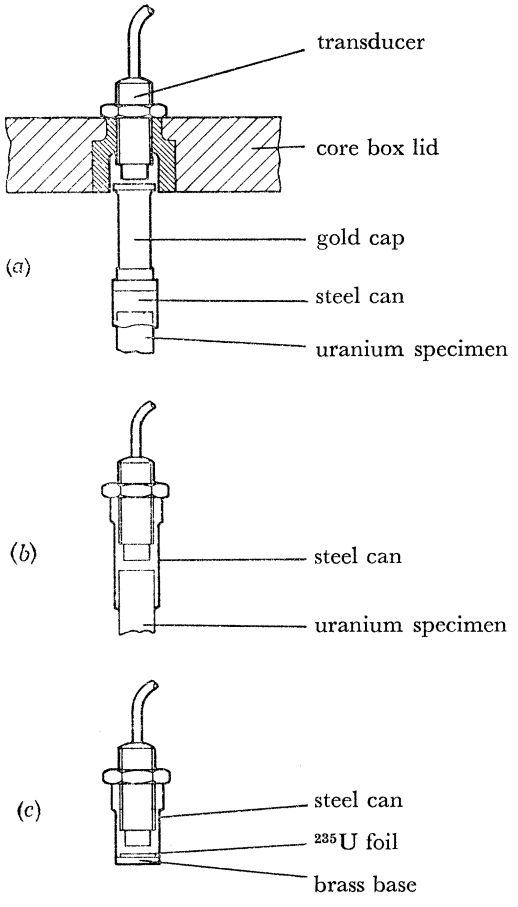

FIGURE 14. Arrangement of proximity transducers.

The probes were calibrated by rotating their mounting screws (the pitch of the thread being known). Where probes were facing bare uranium, corrosion problems were important, and frequent calibration was necessary.

Usually during a pulse two probes were in use, arranged as in figures 14 (*b*) and (*c*), one measuring displacement plus interference and the other interference. The d.c. outputs from the probes were passed through an analogue-to-digital converter to the store of a Ferranti Argus 500 computer. At a convenient time the data was taken from the store on to 8-track paper tape. A data tape translation was then applied to convert the information to binary Atlas machine code

and an Atlas computer was used to provide synchronization of signals, subtraction of interference, comparison with calibration and finally graphical output. Some trouble was experienced with 'cross-talk' between the f.m. preamplifiers in the two channels, but this was overcome by shielding and the use of low pass filters.

4. Experimental displacements and comparisons with theory

During each of the five reactor pulses used in testing the experimental cylinders and cones, the reactor period $1/\alpha_0$ was measured by using a scintillation counter. For our analytical work we should normally derive ω from α_0 by means of equation (4). However McTaggart *et al.* (1968) have shown that for the shorter Viper pulses the pulse half-width is longer than would be predicted by Wimett's (1960) analysis (see equation (1)). The reason is largely that Wimett's analysis assumes that μ, the temperature coefficient of reactivity, is a constant. This is probably true for the fuel rod expansion component of μ, but it is not true for the Doppler component, which varies with temperature. McTaggart *et al.* (1968) suggest (see their table 4) that for $1/\alpha_0$ around 105 μs, ω should be decreased by a factor 1.31, or 1.25 for 115 μs.

Readings of thermocouple ET 10 during the pulses enabled the specimen maximum temperature rises to be determined (see § 3.1) and thence the average specimen temperatures during each pulse. These varied from 92 to 185 °C. Our analysis does not allow for variation of Young's modulus with temperature and so we have to choose some average value. From the results of table 3 a value of $E = 140\,\mathrm{GN/m^2}$ will be taken as sufficiently accurate for all of the pulses: it is not believed that the increase in strain rate from the materials tests (< 0.25/s) to the pulses (up to 10/s) will have any significant effect upon E (Maiden (1959)).

The parameters appropriate to each of the experimental pulses are given in table 4 below. Details of the specimens were given previously in table 2 and of the temperature distributions in figure 13.

Table 4. Pulse and specimen parameters

specimen	α_0^{-1} / μs	ω / s^{-1}	B	C	corrected ET 10† / K	max. temp rise / K
1	105	5710	0.0487	∞	187	374
2	105	5710	0.0886	∞	189	166
3	115	5460	0.0848	∞	179	322
4	106	5650	0.0878	0.47	183	161
5	103	5820	0.0903	0.47	197	355

Theoretical end displacements of the specimens, using the data of table 4 and figure 13 in equation (17) are given in figures 15 to 19 together with the experimental results. The time zero for the experimental curves is the firing of the accelerator source; that for the theoretical curves is of course arbitrary.

Figure 15 shows the results for the fuel rod in the core. As we should expect with a value of B less than 0.05 there is no discernible oscillation (see figure 6). The theoretical displacement starts later and finishes sooner than the experimental curve. The difference is largely accounted for by our choice of displacement function, since the experimental curve fits equation (2) better than equation (3)—see figure 4.

† The reading of ET 10 is subject to a small correction for the heating between the end of the pulse and the time when the safety blocks are driven out (see § 1).

PHILOSOPHICAL TRANSACTIONS OF THE ROYAL SOCIETY A MATHEMATICAL, PHYSICAL & ENGINEERING SCIENCES

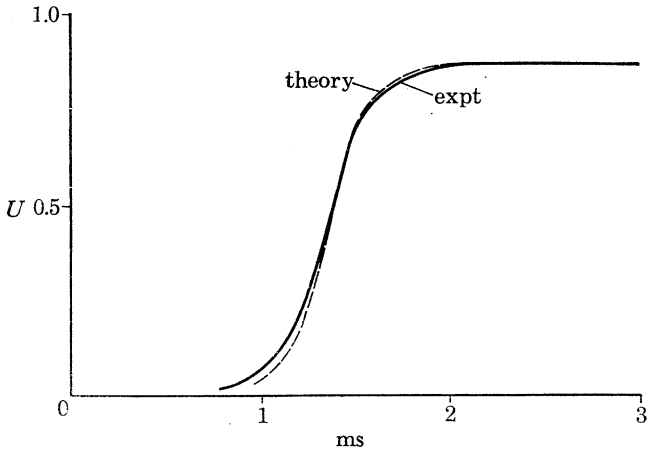

FIGURE 15. End displacement of fuel rod. $\omega = 5710/s$, $B = 0.0487$; max. temp. rise = 374 K.

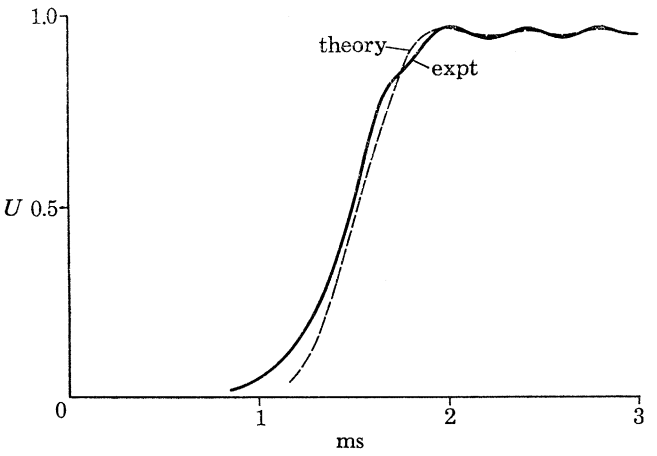

FIGURE 16. End displacement of cylinder. $\omega = 5710/s$, $B = 0.0886$, max. temp. rise = 166 K.

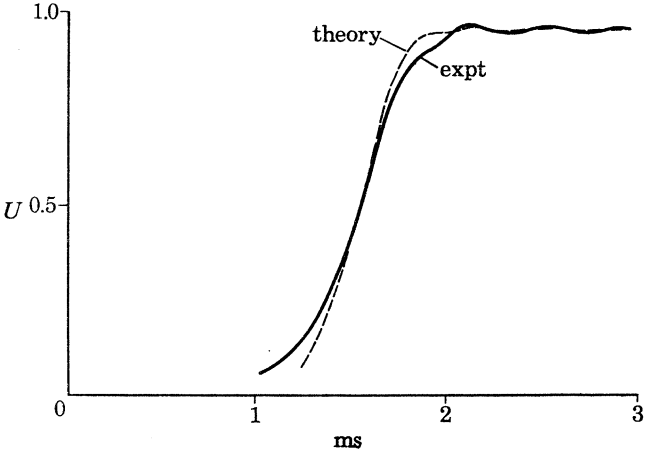

FIGURE 17. End displacement of moderated cylinder. $\omega = 5460/s$, $B = 0.0848$, max. temp. rise = 322 K.

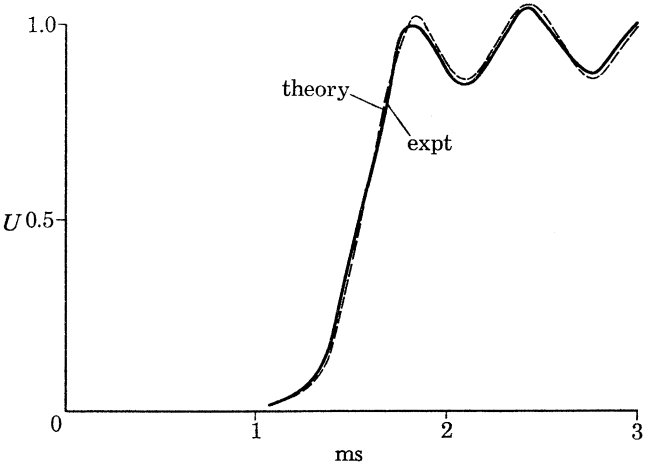

FIGURE 18. End displacement of cone. $\omega = 5650/s$, $B = 0.0878$, max. temp. rise = 161 K.

Figure 16 gives the results for the cylinder in the cavity. With a value of B of 0.0866 we should expect a small oscillation (see figure 6). The theoretical amplitude of oscillation is less than that measured experimentally, but no close agreement should be expected here, since the theoretical results are very sensitive to the precise value of B (the amplitude is near a zero at $B = \frac{1}{12}$: see § 2.2). What is of more significance is the excellent agreement on frequency of oscillation, since this confirms the low value for the Young modulus which we have been using. The same general remarks apply to the rising part of the curves as to figure 15, but the experimental curve in figure 16 also shows a 'shoulder' just before the oscillatory portion which is not predicted by the analysis. This discrepancy again seems to be associated with the difference between equation (2) and (3), since a numerical analysis based on Hansen's equation does predict the shoulder. Figure 17 shows the results for the moderated cylinder in the cavity. The same comments apply as to figure 16.

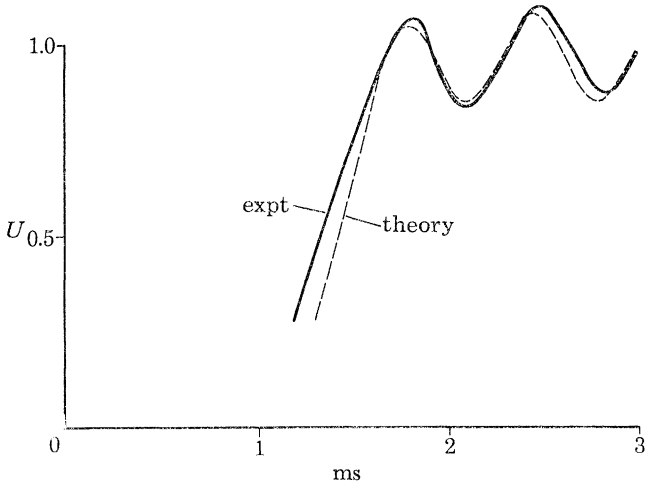

FIGURE 19. End displacement of moderated cone. $\omega = 5820$/s, $B = 0.0903$, max. temp. rise = 355 K.

The results for the cone are given in figure 18. Agreement between the theoretical and experimental curves is very close. Again, the concurrence of the theoretical and experimental frequencies of oscillation provides confirmation of our value for the Young modulus. Figure 19 shows the results for the moderated cone. Agreement between theory and experiment is not quite as good as for the previous case, probably because the assumed temperature distribution is not quite correct near the encastred end (see § 3.1).

The authors would like to express their thanks to the United Kingdom Atomic Energy Authority for the provision of experimental facilities and for the manufacture of the test specimens.

REFERENCES

Adamson, P., Norman, S. & Picton, G. 1969 The effects of hydrogen on the tensile properties of uranium when tested in different environments. *J. nucl. Mater.* **33**, 215–224.

Austin, A. L. & Parker, R. 1967 Determining the dynamic elastic modulus at elevated temperatures by using rapid heating techniques. *J. bas. Engng Trans. ASME* (Series D) **89**, 1, 111–115.

Chadwick, P. 1962 On the propagation of thermoelastic disturbances in thin plates and rods. *J. Mech. Phys. Solids* **10**, 99–109.

Danilovskaya, V. I. 1950 Temperature stresses in an elastic half-space arising as a consequence of the sudden heating of its boundary. *Prikl. Mat. Mekh.* **14**, 316–318.

Danilovskaya, V. I. 1952 On a dynamical problem in thermoelasticity. *Prikl. Mat. Mekh.* **16**, 341–344.
Eason, G. & Sneddon, I. N. 1959 The dynamic stresses produced in elastic bodies by uneven heating. *Proc. R. Soc. Edinb.* A **65**, 143–176.
Gittus, J. H. 1963 *Uranium.* London: Butterworths.
Glasstone, S. & Edlund, M. C. 1953 *The elements of nuclear reactor theory.* London: Macmillan.
Gow, J. D. & Pollock, H. C. 1960 Development of a compact evacuated pulsed neutron source. *Rev. scient. Instrum.* **31**, 235–240.
Hansen, G. E. 1952 Burst characteristics associated with the slow assembly of fissionable materials. Los Alamos Scientific Laboratory, LA-1441.
Hegemier, G. A. & Morland, L. W. 1967 Stress waves in a temperature dependent viscoelastic half-space subjected to impulsive electromagnetic radiation. University of California, San Diego, AFOSR 67-2453.
Jeffreys, H. 1930 The thermodynamics of an elastic solid. *Proc. Camb. Phil. Soc.* **26**, 101–106.
Kenner, V. H. & Goldsmith, W. 1968 Elastic waves in truncated cones. *Proc. Soc. exp. Stress Analysis* XXV(**2**), 442–449.
Krawarik, P. & Sexl, R. 1966 Thermally excited rod oscillations. *Acta phys. austriaca* **24**(4), 337–352.
Landon, J. W. & Quinney, H. 1923 Experiments with the Hopkinson pressure bar. *Proc. R. Soc. Lond.* A **103**, 622–643.
Lessen, M. 1956 Thermoelasticity and thermal shock. *J. Mech. Phys. Solids* **5**, 57–61.
Lessen, M. 1957 The motion of a thermoelastic solid. *Q. appl. Math.* **15**, 105–108.
McIntosh, A. B. & Heal, T. J. 1958 High temperature properties of uranium and its alloys. *Proc. 2nd Int. Conf. on Peaceful Uses of Atomic Energy*, Geneva, **6**, 413–425.
McTaggart, M. H., Goodfellow, H., McCormick, W. B. & Weale, J. W. 1968 The fast pulsed reactor VIPER, Part 2. *J. Br. nucl. Energy Soc.* **7**, 328–342.
Maiden, C. J. 1959 The strain-rate sensitivity of α-Uranium. *J. Mech. Phys. Solids* **7**, 106–113.
Michaels, J. E. 1958 Thermally induced elastic wave propagation in slender bars. *3rd U.S. Nat. Congr. Appl. Mech.* pp. 209–213.
Morland, L. W. 1969*a* Elastic-plastic wave generation by impulsive electromagnetic radiation. *Int. J. Solids Structs* **5**, 319–333.
Morland, L. W. 1969*b* Plastic yield and reverse yield waves generated by impulsive electromagnetic radiation. *Int. J. Solids Structs.* **5**, 843–853.
Percival, C. M. & Cheney, J. A. 1969 Thermally generated stress waves in a dispersive elastic rod. *Proc. Soc. exp. Stress Analysis* XXV1(**1**), 49–57.
Randles, J. 1966*a* Feedback due to elastic waves and Doppler coefficient during the excursions of a pulsed fast reactor. *J. nucl. Energy* (A/B) **20**, 1–16.
Randles, J. 1966*b* Accident and self-regulation studies of pulsed fast reactors. *J. nucl. Energy* (A/B) **20**, 713–728.
Randles, J. & Jaarsma, R. 1967 Some problems of stress wave production encountered in the study of pulsed fast reactor dynamics. *Euratom Report* 3654*e*.
Renner, S. S. & Sharma, O. P. 1966 Interaction of laser radiation with an absorbing semi-infinite solid bar. *J. appl. Phys.* **37**, 2304–2308.
Rogge, T. R. 1970 Longitudinal waves in circular conic sections. *S.I.A.M. J. Appl. Math.* **19**, 532–541.
Serdyukova, S. I. 1970 Thermoelastic stresses in a circular cylinder. *Joint Institute for Nuclear Research, Dubna.*
Sneddon, I. N. 1959 The propagation of thermal stresses in thin metallic rods. *Proc. R. Soc. Edinb.* A **65**, 121–142.
Suvorov, Iu. P. 1963 The propagation of thermal stresses in a elastic-plastic bar. *Prik. Mat. Mekh.* **27**(2), 383–389.
Suvorov, Iu. P. 1964 On the propagation of elastic-plastic waves during heating of a semi-infinite bar. *Prik. Mat. Mekh.* **28**(1), 91–98.
Weale, J. W., Goodfellow, H., McTaggart, M. H. & Warnke, E. G. 1968 The fast pulsed reactor VIPER, Part 1. *J. Br. nucl. Energy Soc.* **7**, 313–327.
Wimett, T. F., White, R. H, Stratton, W. R. & Wood, D. P. 1960 Godiva II—an unmoderated pulse-irradiation reactor. *Nucl. Sci. Engng* **8**, 691–708.
Zaker, T. A. 1965 Stress waves generated by heat addition in an elastic solid. *J. appl. Mech.* **32**, 143–150.

PHILOSOPHICAL TRANSACTIONS OF THE ROYAL SOCIETY A MATHEMATICAL, PHYSICAL & ENGINEERING SCIENCES

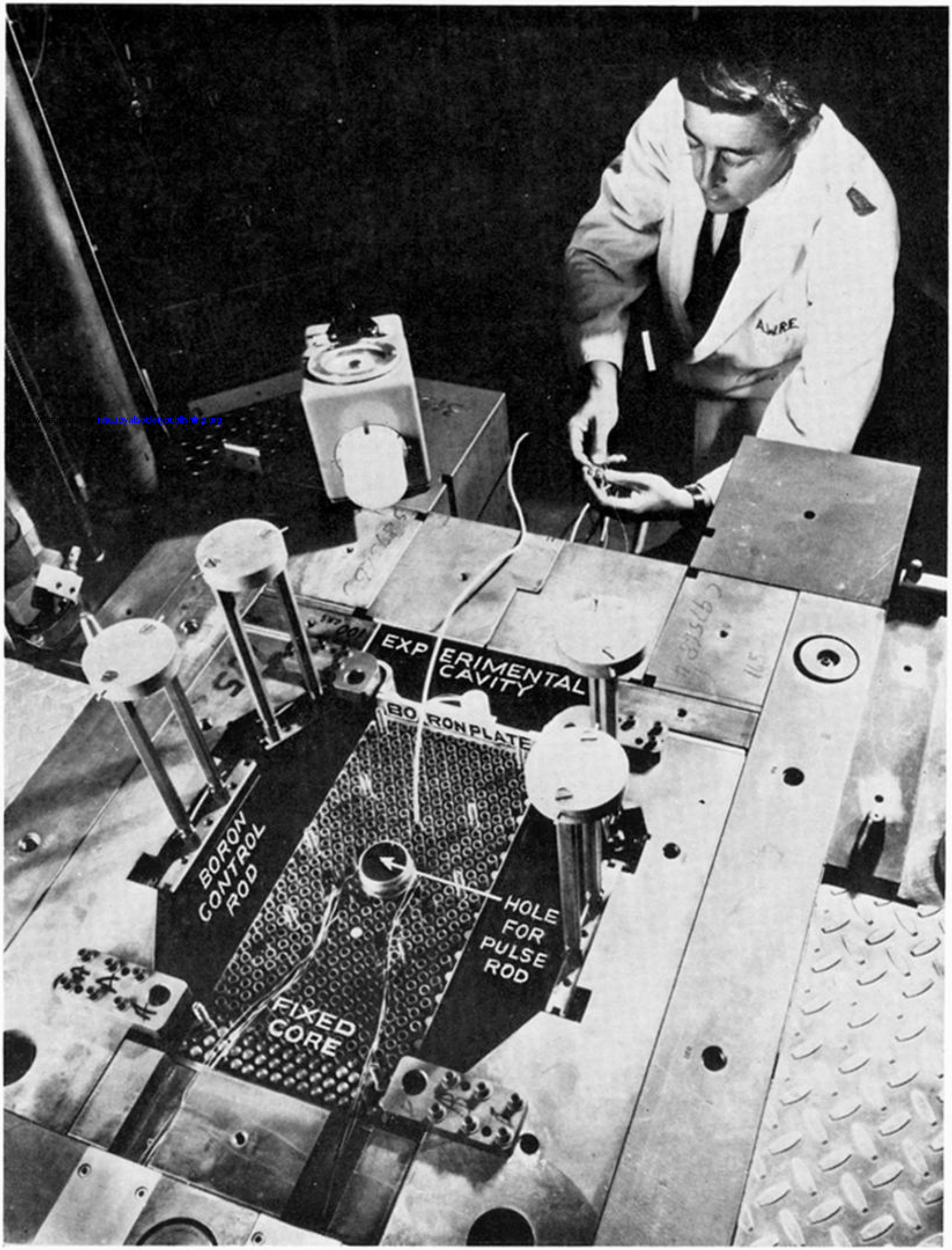

IGURE 3. Reactor core with reflector top and core box lid removed and the safety blocks lowered.

(U.K.A.E.A. Copyright)